Electric Power Components and Systems, 30:705–721, 2002

1532-5008/02 $12.00 + .00
DOI: 10.1080/15325000290085136

A Novel Design of Optimal Phase Current Waveform for an Electric Vehicle Wheel Motor

YEE-PIEN YANG
YIH-PING LUH
CHI-MING LEE

Department of Mechanical Engineering
National Taiwan University
No. 1, Roosevelt Road, Sec. 4
Taipei, Taiwan 106, R.O.C.

A novel design of optimal current waveform for a disc-type axial-flux wheel motor is presented in this paper. This dedicated wheel motor has been designed and installed directly inside the wheel of electric vehicles without mechanical differentials and reduction gears. The torque-oriented optimization is performed to obtain the optimal current waveform subject to various constraints for independent winding structure. The best one of the optimal waveforms for maximized torque with confined ohmic loss is found to be proportional to the magnetic flux variation in the air-gap between the stator and the rotor.

Keywords axial-flux wheel motor, optimal driving waveform, electric vehicle

1. Introduction

Electric vehicles (EVs) have played an important role in the protection of natural environment. Traditional power systems of EVs consist of batteries, electric motors with drives, and transmission gears to wheels. Each subsystem converts chemical, electrical, or mechanical energy into different forms, thus consuming energy through the dissipation components of windage and friction. Researchers and engineers are looking for various approaches to improve the overall efficiency of electric vehicles, and hence to increase their driving range. In addition to new battery technologies, new concepts for the design of motor and their optimal driving pattern have attracted substantial attention for the improvement of overall efficiency and reliability of EVs.

One of the new motor designs used in this paper is the wheel or hub-in motor directly mounted inside the wheel, thus eliminating transmission gears or mechanical differentials with their associated energy loss. In addition, the reduction of mechanical components in transmission chains or gears not only improves over-

Manuscript received in final form on 30 July 2001.
The authors acknowledge the financial support of the National Science Council of Taiwan, Republic of China, under Contract No. NSC88-2622-E-002-003.
Address correspondence to Prof. Yee-Pien Yang. E-mail: ypyang@ccms.ntu.edu.tw

all efficiency but also reduces vehicle weight. Various axial-flux wheel motors have been proposed for electric cars [1–4]. Lacking reduction gears, mechanical transmission, and differential, most wheel motors need large input current to develop large torque at low speed operation; however, greater ohmic loss, which is proportional to the square of current, caused inevitable reduction of efficiency. Therefore, a proper driving current pattern is one of critical solutions in increasing the EV's efficiency.

Optimal control waveforms have attracted considerable attention from researchers and engineers for a variety of electric motors. In order to produce maximum torque per stator current at various operating conditions, Ohm [5] developed an algorithm to find the optimal advance angle of the desired stator current command for PM synchronous motors. Verl and Bodson [6] discussed torque maximization for PM synchronous motors in the presence of voltage and current constraints throughout the low-, intermediate-, and high-speed regions. Low et al. [7] proposed a motor identity modeling approach to determine the optimal current profile to maximize torque for driving the permanent magnet synchronous motor. A system of two-loss model controllers was proposed by Mademlis et al. [8] to determine the optimal air-gap flux and the optimal excitation current to minimize losses; however, most optimal current waveforms were based on the conventional assumption of motors that their back emf was square, trapezoidal, or sinusoidal due to the lack of design information on the shape of the magnetic field flux distribution in the air gap between the rotor and the stator.

This paper presents a novel approach for determining the optimal current pattern for the disc-type axial-flux brushless DC wheel motor by maximizing the output torque with respect to the rotor shift. In terms of original design parameters, the magnetic circuit model of the customized motor is established. The air gap characteristics, such as torque, flux, and its variation, are described as functions of rotor shift. The field flux variation, and hence the back emf, is not anymore a regular function of sine, square, or trapezoid. The resulting optimal current waveform is proved by Cauchy-Schwarz inequality and is verified numerically through optimization schemes with various constraints. Finally, the plan of implementation proposes a novel sensor structure for current switching and for precise tracking of the optimal current pattern stored in a digital signal processor.

2. Axial-Flux Wheel Motor

2.1. Specification

The dedicated disc-type axial-flux brushless DC wheel motor presented in this paper is a prototype for electric vehicles, as developed in the Electro-mechanical Power System Research Group at National Taiwan University. The cross-sectional view, explosive graph, and prototype of the wheel motor are illustrated in Figure 1, and its primary components and specifications are listed in Table 1. Figure 1 shows diagrammatically a non-salient-pole rotor disc of the hub-in motor with 16 magnets of two flat surfaces to form 16 poles, and it is sandwiched between two plates of stator, each with 24 teeth. This indicates that the slot pitch of two adjacent slots is 2/3 pole pitch, and the number of slots per pole per phase is 1/2. This fractional pitch arrangement yields a uniform magnetic force distribution between the stator and the rotor, hence eliminating most of the cogging torque that usually occurs in permanent-magnet motors. The ND27SH NbFeB magnet is used, which has

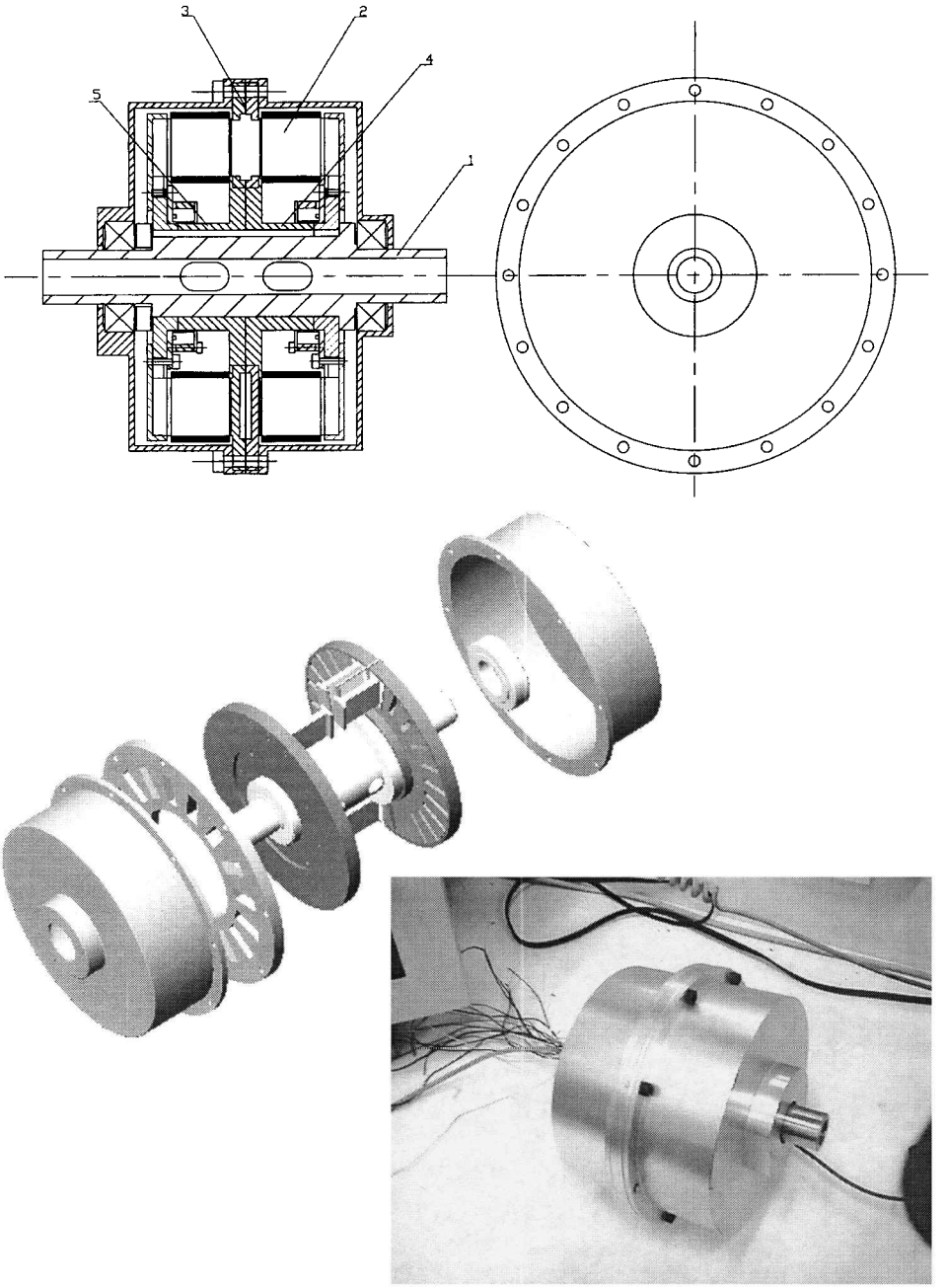

Figure 1. The cross-sectional view, explosive graph, and prototype of axial-flux disc-type wheel motor (1-wheel axle, 2-stator teeth, 3-rotor disk, 4/5-positioning axle sleeve).

Table 1
Motor specifications

Overall ratings	
Rated speed: 450 rpm	Max. speed: 1200 rpm
Rated current: 96 A	Max. current: 144 A
Rated torque: 3.2 kg-m	Max. torque: 6 kg-m
Rated voltage: 15 V	Max. voltage: 48 V
Rated power: 1.5 kW	Max. power: 3.0 kW
Geometric dimensions	
Outer radius: 89 mm	Inner radius: 60 mm
Air gap length: 0.5 mm	Number of coils per tooth: 130
Number of phase: 3	Coil diameter: 0.6 mm

remanence of 1.05 Tesla and coercivity of 9.5 kOe. The laminated electric steel sheets 35RM230 (0.35 mm) have core loss of 2.2 W/kg at 1 Tesla and 100 Hz, and their saturation flux density is between 1.4 and 1.9 Tesla. The tire is installed on the outer case rotating with the rotor. The main magnetic flux flows through two air-gaps between the stator and rotor along the axial direction.

The final shape of this wheel motor is designed to meet required specifications of a multifunctional optimization scheme, with various constraints, such as limited space, current density of conductor, flux saturation, and driving voltage. Instead of being Y-connected, the coils are independently wired on stator poles and are grouped into three phases. Independent winding structure is one of the features of this dedicated wheel motor, in which the stator coils are independently wound and bound into required phases. Since there is no neutral point for independent winding, the driving voltage is directly applied to each phase. Therefore, larger back electromotive force is induced and higher motor speed can be reached.

2.2. Magnetic Circuit Model

The torque of electric motors is produced by the rate of change of the magnetic energy stored in the air-gap. The magnetic energy comes out from the magnetic field created by the current flowing in the wires and/or permanent magnets. Both sources generate magnetic flux forming flux loops in the magnetic materials of the motor. Based on the assumptions of material linearity and the collinearity of flux and field densities, the magnetic circuit model is used to describe the torque produced in the motor. It is also necessary to make three additional assumptions:

(1) The motor is operated in the linear range of the B-H curve of magnetic materials.
(2) The air-gap reluctance of the slotted stator structure is approximated by effective air-gap length with Carter's coefficient [9].
(3) The flux flows straight across the air-gaps between the stator and rotor, namely, the overlapping area method, ignoring the fringing flux for simplified analysis.

The field coenergy within the air-gap of the axial-flux wheel motor is expressed in the form

$$W'(\theta) = \frac{1}{2} \sum_{i=a,\,b,\,c} [(R_{gi} + R_P)\phi_{P\,i}^2 + L_i I_i^2 + 2N\phi_{P\,i} I_i], \tag{1}$$

where N is the number of turns per tooth, R_{gi} is the air-gap reluctance corresponding to the coil winding phase i, R_P is the magnet reluctance, $\phi_{P\,i}$ is the magnet flux flowing through coil winding phase i, and L_i and I_i are the self-inductance and exciting current of coil winding phase i, respectively. It is apparent that R_{gi}, $\phi_{P\,i}$, and L_i are functions of rotor shift (i.e., the relative angular position of rotor and stator) but R_P is not. The total torque consisting of cogging, reluctance, and alignment torques is obtained from the rate of change of the field coenergy in a linear operation range as follows:

$$T = \frac{\partial W'(\theta)}{\partial \theta} = \frac{1}{2} \sum_{i=a,\,b,\,c} \left[-\frac{dR_{gi}}{d\theta}\phi_{P\,i}^2 - \frac{dR_i}{d\theta}\phi_{C\,i}^2 + 2NI_i \frac{d\phi_{P\,i}}{d\theta} \right], \tag{2}$$

where $\phi_{C\,i}$ is the flux produced by coil i flowing through the air-gap and rotor magnets and R_i is composed of air-gap and rotor magnet reluctances through which $\phi_{C\,i}$ flows. The second term is the other expression of the reluctance torque due to the fact $L_i I_i^2 = R_i \phi_{C\,i}^2$ [10].

In the above expression, the first term is the cogging torque produced by the rotor magnets, which is the rate of change of the stored magnetic energy in the air-gap between stator teeth and rotor poles. As this portion of torque is evaluated, the stator coils are not excited by phase currents but linked with the flux flowing out of rotor magnets. The second term represents the reluctance torque occurring whenever the air-gap reluctance is decreasing and the inductance associated with coils is increasing. Regardless of the flux from magnets, this torque component is calculated only with the flux produced by coils, and its peak ratio is less than 0.5% of the gross torque of the dedicated wheel motor. The third term in (2), called mutual or alignment torque, happens as the mutual flux links the magnet to the coil. This is the primary torque component of a brushless DC motor.

The 3D motor structure can be simplified to a 2D configuration, as shown in Figure 2, for facilitating the magnetic circuit analysis. The laminations of the stator are composed of sheets of electric steel and are oriented in a stack coming out of the paper. In a section of 360 electrical degrees, the magnetic circuit of one flux loop is composed of three teeth on each side of the stator facing toward two permanent magnets embedded in the rotor. As a matter of fact, the ferromagnetic material has very high permeability and its reluctance can be ignored. Figure 3 shows that the magnet flux splits into the stator teeth from one side and returns from the other side, the air gap reluctance facing each stator tooth varies with the rotor shift [10]. For example, R_{gal} is a variable air gap reluctance corresponding to left branch of the flux splitting into phase a, and similar definitions are used for R_{gbl} and R_{gcl}. Moreover, $2R_{ml}$ denotes the flux leakage reluctance from magnet to magnet, and ϕ_r denotes the flux source of a magnet with reluctance R_m. Through basic electrical and mechanical relationships, the air gap flux corresponding to phase i along the left branch of the circuit is expressed as

$$\phi_{P\,il}(\theta) = \frac{1/R_{gal}}{1/R_{gal} + 1/R_{gbl} + 1/R_{gcl}} \phi_m, \quad i = a, b, c, \tag{3}$$

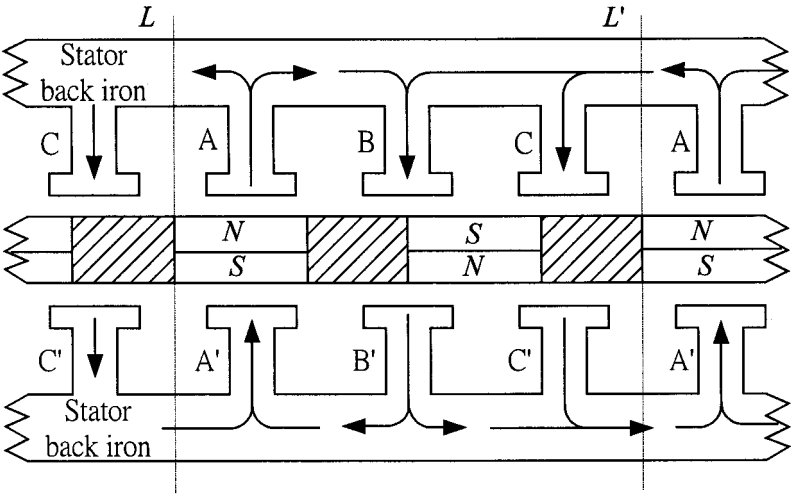

Figure 2. Two-dimensional motor structure in 2π electric angle ($L - L'$).

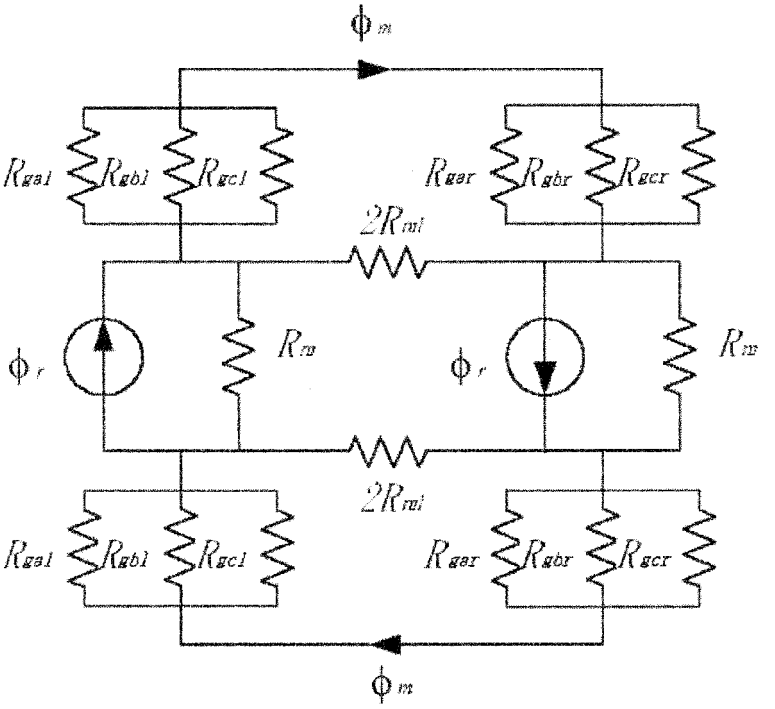

Figure 3. Magnetic circuit model for the wheel motor in 2π electric angle.

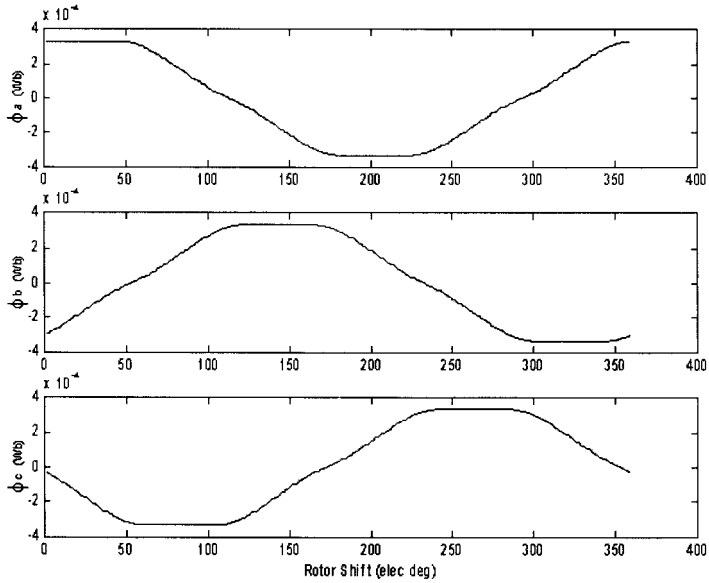

Figure 4. Air gap flux in three phases.

where $\phi_{P\,il}$ is a function of the rotor shift θ and ϕ_m is the magnet flux leaving the magnet and crossing the air gap. Similar expressions hold for the right branch of the circuit. In that way, the summation of fluxes corresponding to three phases at any rotor shift is equivalent to the total air gap flux in one magnetic loop. Subscript omission for left and right branch yields

$$\phi_{P\,a} + \phi_{P\,b} + \phi_{P\,c} = \phi_m \,. \tag{4}$$

In other words, at any rotor shift, the magnet flux crossing the air gap finds its way getting into three phase coils and completes a loop. Figure 4 shows the magnetic flux distributions that vary periodically in the air gap between the stator and rotor, and the air gap flux variations in three phases are depicted in Figure 5.

3. Optimal Current Waveform

Since the cogging torque, which is inherent from the original design of the motor, is independent of driving currents, and the reluctance torque is small enough to be neglected, the optimal current waveform is then determined by maximizing the alignment torque in the sense of average. The statement of optimization is described as follows:

The average torque is maximized under a constraint on the average ohmic loss. Hence, the performance index can be expressed as

$$T_{A,avg} = \frac{1}{2\pi}\int_0^{2\pi} T_A(\theta)d\theta \tag{5}$$

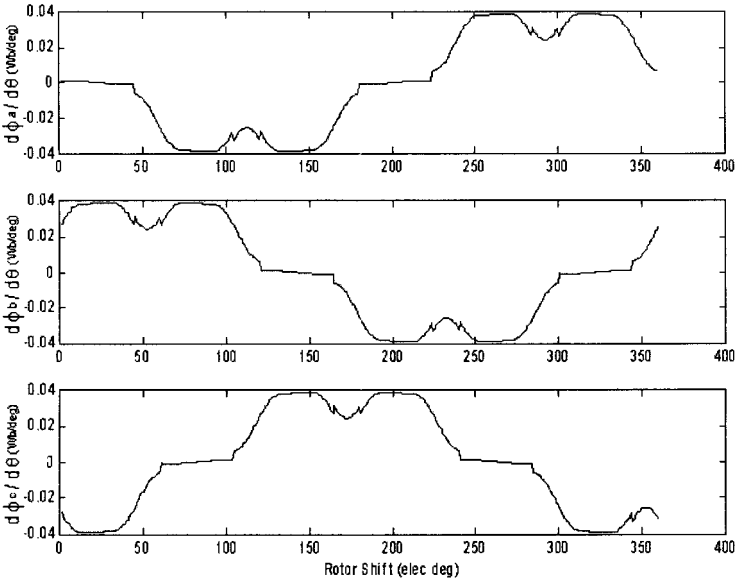

Figure 5. Air gap flux variations in three phases.

subject to the constraint

$$\int_0^{2\pi} I_i^2 d\theta \leq \int_0^{2\pi} 6^2 d\theta, \quad i = a, b, c, \tag{6}$$

where

$$T_A(\theta) = \frac{1}{2} \sum_{i=a,b,c} N I_i(\theta) \frac{d\phi_{P\,i}(\theta)}{d\theta}. \tag{7}$$

Both theoretical and numerical analyses are made for the optimal current waveform with the following assumptions. First, the motor is operated under the rated speed so that the back-emf induced in each phase of the motor must not exceed the driving voltage. Second, the limitation of current and power loss of the conductor is released, which was prescribed by the maximum allowable current density of the conductor due to its cross section.

3.1. Theoretical Analysis

Theoretically, the optimal current waveform is analyzed by maximizing the torque in the sense of average. In equations (5) and (7), the alignment torque T_A, the magnet flux $\phi_{P\,i}$, and the current input I_i flowing through coil winding phase i are all functions of rotor shift θ. The average torque T_A over an electric period can be calculated approximately in a summation of n points and expressed as

$$T_{A,avg} = \frac{1}{2} \sum_{i=a,b,c} N \left[\frac{1}{n} \sum_{j=1}^{n} I_i(j) \frac{d\phi_{P\,i}(j)}{d\theta} \right]. \tag{8}$$

From the Cauchy-Schwarz inequality [11] for sums

$$\left(\sum_{j=1}^{\infty} |a_j b_j|\right)^2 \leq \left(\sum_{k=1}^{\infty} a_k^2\right)\left(\sum_{m=1}^{\infty} b_m^2\right), \tag{9}$$

the maximum value of the left-hand-side summation occurs when the following relationship exists:

$$\frac{a_1}{b_1} = \frac{a_2}{b_2} = \frac{a_3}{b_3} = \cdots = c, \tag{10}$$

in which c is a nonzero constant. Likewise, the maximum average torque takes place when $I_i(j)$ and $\frac{d\phi_{P\,i}(j)}{d\theta}$ are proportional.

This result reveals the following fact:

> *The maximum torque for the brushless DC motor is obtained by the current input with the same waveform as the flux variation in the air-gap between the stator and the rotor. In other words, the phase of the stator current to produce a maximum torque must have 90 electrical degrees from the permanent magnet flux angle of the rotor. In terms of the rotating d-q axis fixed on the rotor [12], the control vector has no component in the direct axis, along which the flux is purely supplied from the permanent magnet [5].*

3.2. Numerical Analysis

In this stage, we will not only verify numerically the optimal current waveform through numerical optimization analysis, but also compare the motor performance with rectangular currents usually applied for brushless DC motors with trapezoidal back emf. The optimizer "constr" in MATLAB is used for maximizing either the average torque (5) over an electric period, or the torque (7) at each point in terms of rotor shift. The design variable is current, which is optimized, point by point at discrete rotor shifts, or is expressed as a current function and optimized iteratively over an electrical period.

In the following optimization process, the constraint on the maximum terminal voltage per phase is given as

$$\omega_e \frac{d\lambda_i}{d\theta} + R_{P\,H\,i} I_i < 48V, \quad i = a, b, c, \tag{11}$$

where ω_e is the voltage wave speed and λ_i is the flux linkage to the phase winding resistance $R_{P\,H\,i}$. This relation illustrates that the back-emf induced in the motor must not exceed the driving voltage, 48 V; however, for the operation under the rated speed as assumed in the proceeding analysis, this constraint is trivial.

The sequential quadratic programming optimization method in MATLAB is applied to search for the optimal current pattern for each phase. The optimizer assembles the penalty and constraint functions with Lagrange multipliers and searches the stationary point of the Lagrangian function by Newton's method. Thus, it is referred to as the *Lagrange-Newton* method. This method requires initial estimates for Lagrange multipliers and design variables I_a, I_b, and I_c. Their optimization statements are presented as follows.

Case I: The maximum torque for each relative position of rotor and stator is produced under the constraint of current limit. In another way, the maximum torque is calculated point by point at each rotor shift where the discrete current is the design variable. Therefore, the performance index is a function of rotor shift θ and is expressed as (7) subject to the constraint

$$|I_a, I_b, I_c| < I_{\max}\text{amp}, \tag{12}$$

where $I_{\max}$ is limited at 6 amperes by the cross-section of conductor. This yields an optimal current of rectangular waveform with optimal switching angles.

Case II: The average torque is maximized under a constraint on the average ohmic loss. In this case, the design variable is the current function of rotor shift over an electrical period. Hence, the performance index is expressed as (5) subject to the constraint

$$\int_0^{2\pi} I_i^2 d\theta \leq \int_0^{2\pi} I_{\max}^2 d\theta, \quad i = a, b, c. \tag{13}$$

This constrains the ohmic loss during an electric period with no limit on the peak current, and thus resulting in a nonrectangular current waveform.

Case I results in an optimal current of rectangular waveform with optimal switching angles at specific rotor shifts, as depicted in Figure 6, in which all the phase currents reach to their limit of 6 amperes as the six-step driving current. The optimal current waveform in Case II, as the theoretical analysis proved, is indeed proportional to the flux variation in the air gap as shown in Figures 5 and 7, in which the peak current is 8.5 amperes. Moreover, its average torque of 7.8 kg-m is larger than that of 6.5 kg-m produced by the optimal current of rectangular waveform, as illustrated in Figure 8. Although their torque ripples are not trivial, they usually are filtered through mechanical inertia.

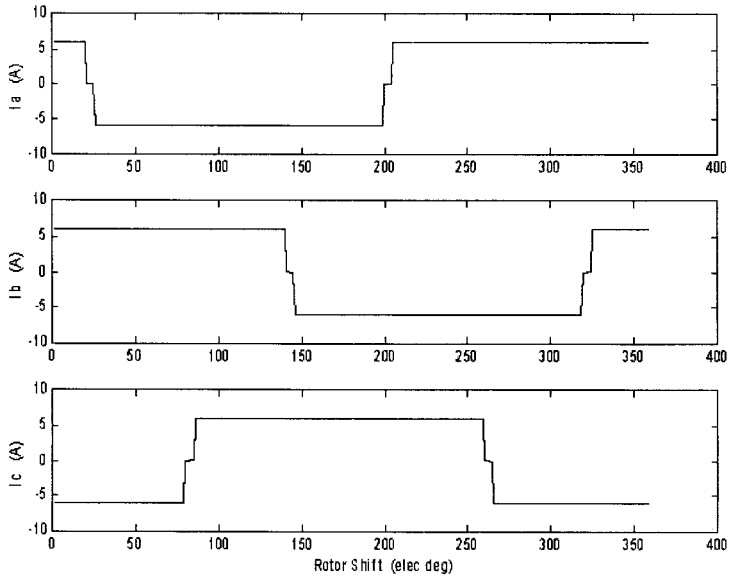

Figure 6. Rectangular current with optimal switching angles.

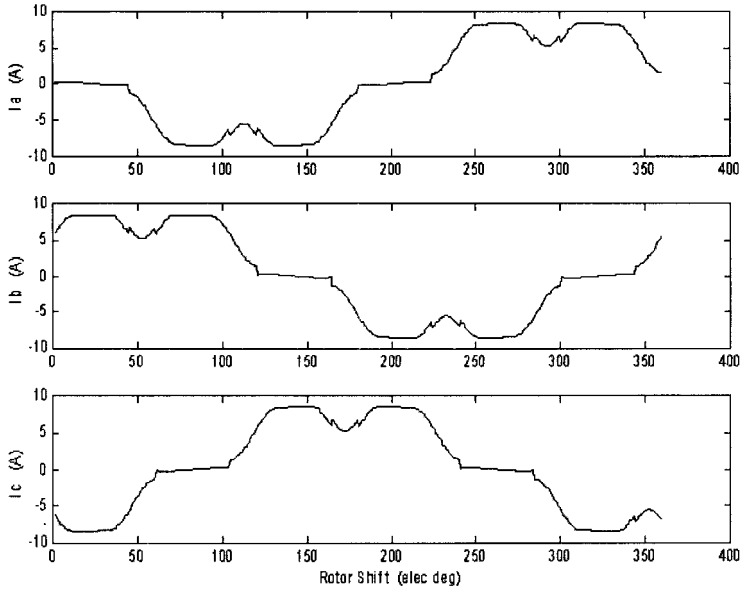

Figure 7. Optimal current with ohm loss constraint.

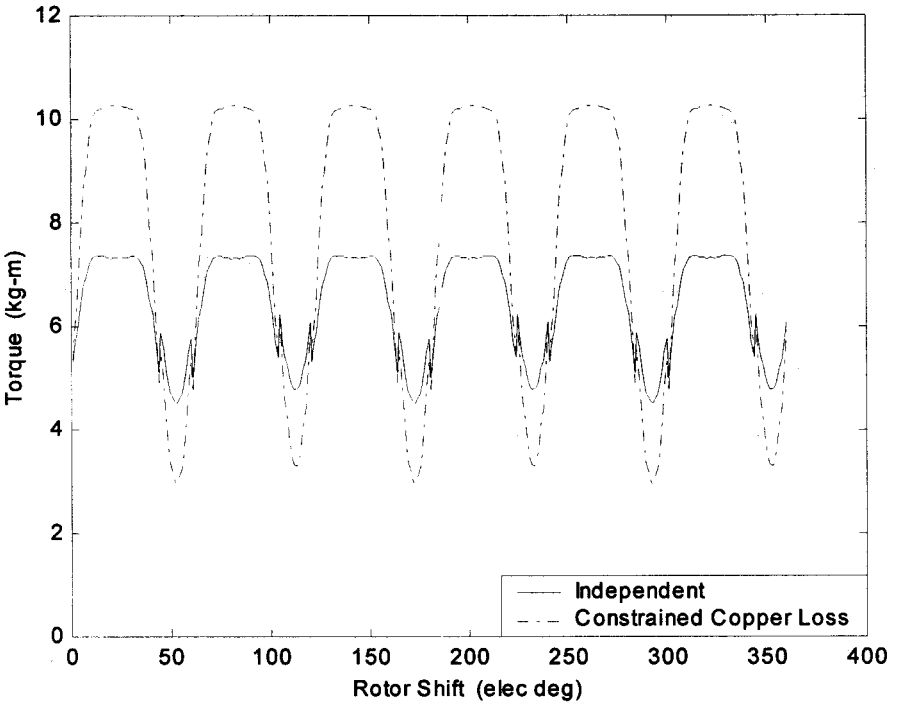

Figure 8. Torque produced by (a) optimal rectangular current pattern (solid curve) and (b) optimal nonrectangular current (dashed curve) of independent winding.

Since both the peak current and load torque are different in the above results, a similar basis is necessary for the comparison of motor performances. Two reference bases are then made with an average torque of 5 kg-m and a peak current of 6 amperes. Table 2 depicts various performances for the motor operated at a low speed operation of 100 rpm. In these cases, the motor efficiency is calculated by

$$\eta = \frac{T_{A,avg}\omega}{T_{A,avg}\omega + P_C + P_I + P_S} \cdot 100\%, \tag{14}$$

where ω is the rotor speed, P_C is the copper of ohmic loss, and P_I is the iron loss. The stray loss P_S comprises windage, friction, noise, and other less dominant loss components. These losses are functions of phase current waveforms and are determined approximately by

$$P_C = \sum_{k=a,b,c} \frac{1}{2\pi} \int_0^{2\pi} I_k^2(\theta) R_k \, d\theta, \tag{15}$$

where R_k is the phase resistance

$$P_I = \rho V K f^{\alpha} B_{M\,ax}^{\beta}, \tag{16}$$

where ρ and V are mass density and volume of the stator steel, respectively, f is the dominant frequency of the input current, and $B_{M\,ax}$ is the maximum flux density of the electric steel 35RM230, whose material coefficients are given by $K = 0.0079$, $\alpha = 1.2704$, and $\beta = 1.7008$. The stray loss P_S usually is estimated by the designer and is chosen at 5% of the average output power $T_{A,avg}\omega$ in this paper.

As the result indicates, the efficiencies for Case II with constrained ohmic loss are superior to those for Case I. For the same limit on the peak current, the optimal rectangular current waveform of Case I produces the highest average torque; however, its torque constant is the smallest. In this case, larger torque may be necessary for starting or accelerating operation at lower speed while sacrificing some motor efficiency. For high-speed cruising stage of the electric vehicle, the optimal current waveform proportional to the flux variation becomes a better solution for efficiency, which is shown in Figures 9 to 11 for various load torques.

Table 2
Motor performance by optimal current inputs (100 rpm)

Basis	Average torque load at 5 kg-m		Peak current limit at 6 amperes	
Case	I	II	I	II
Max./Avg. torque (kg-m)	5.7/5.0	6.6/5.0	7.3/6.5	7.3/5.5
Torque ripple (%)	13.8	31.9	13.8	31.9
Torque constant (kg-m/A)	0.023	0.029	0.023	0.029
Max. current per pole (A)	4.7	5.4	6.0	6.0
Ohmic loss (Watt)	408	288	679	700
Iron loss (Watt)	15.9	8.7	24.7	18.6
Stray loss (5%) (Watt)	25.7	25.7	33.1	28.3
Efficiency (%)	53.3	61.4	47.3	58.7

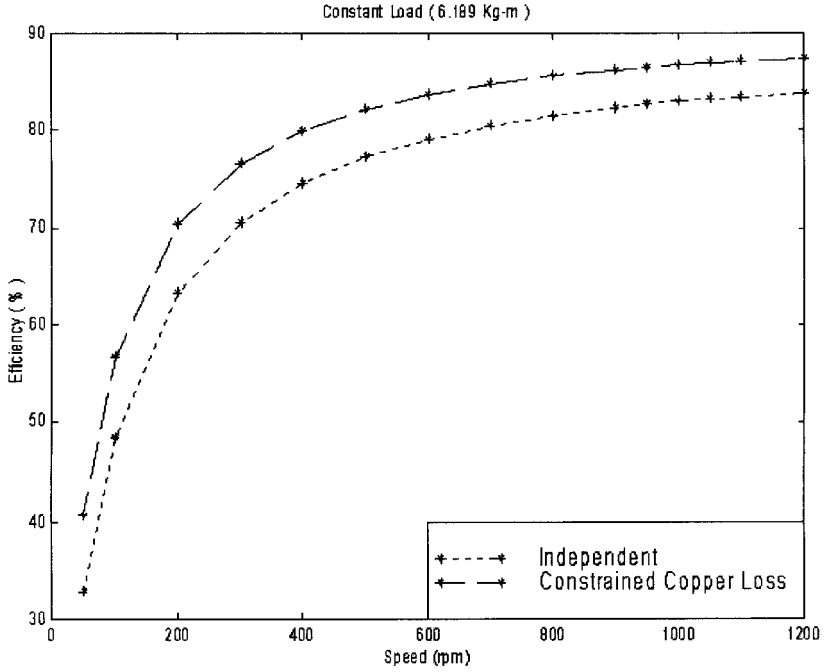

Figure 9. Motor efficiency vs speed under load of 6.2 kg-m.

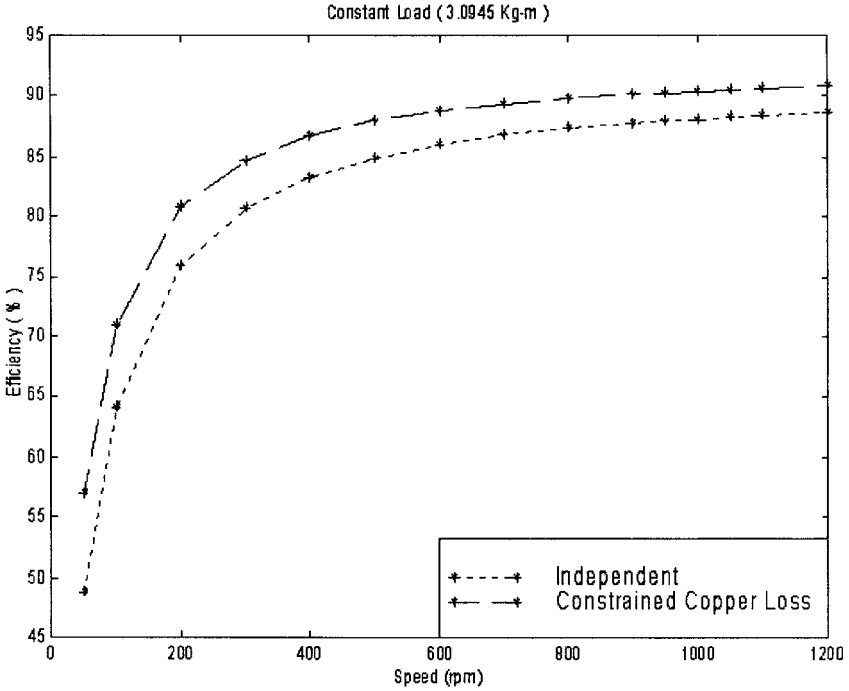

Figure 10. Motor efficiency vs speed under load of 3.1 kg-m.

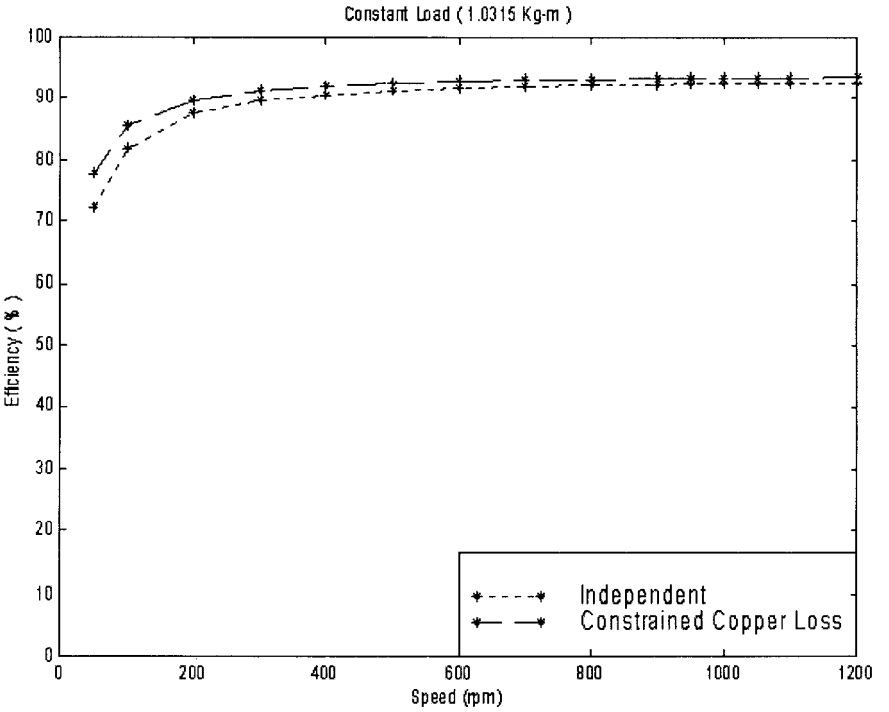

Figure 11. Motor efficiency vs speed under load of 1.0 kg-m.

4. Plan Implementation

To realize the optimal driving current waveform, a motor drive must be designed and implemented. It is not difficult to implement the optimal current of rectangular waveform with specific switching angles; however, it is hard to synthesize, by analogy circuit, the nonrectangular optimal waveform that is proportional to the flux variation. A digital signal processor TMS320F240[1] is then selected to store the optimal current pattern, to process signals, and to create control outputs. The input signals to the processor include a motor acceleration command, rotor shift position signal, and phase current feedbacks. The rotor shift position is sensed by a reflective optosensor, receiving the reflecting light from the black-and-white code belt adhered to the inner side of the rotor. Two kinds of rotor shift positions are critically sensed. One informs the switching point for positive current or negative current and the other one relates the position with the magnitude of the current waveform. Two belts of code are then designed and printed on the transparent plastic paper as shown in Figure 12, where two sets of reflective optosensors, each with three components corresponding to three phases, are located on the stator. One belt consists of eight sets of black-and-white codes. As one of the optosensors receives the forward end of a black belt, the direction of current is changed. The other belt is composed with 720 black-and-white codes so that more precise rotor shifts are sensed and their corresponding current magnitudes

[1]TMS320F240 is a product of TMS320F/C24x series of Texas Instruments.

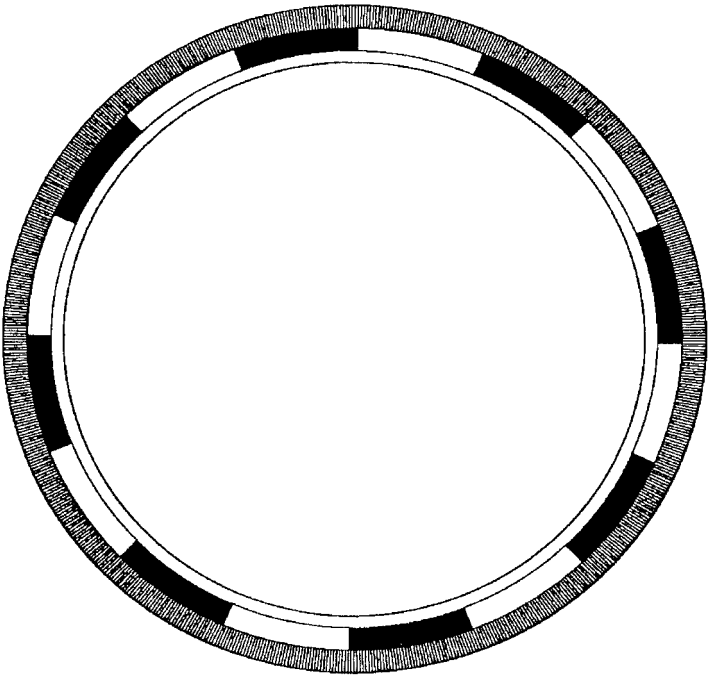

Figure 12. Positioning sensor.

are searched from the digital signal processor, where the optimal current pattern is stored.

The optimal control signals are then generated and converted to pulse-width modulation (PWM) waveforms to the power circuit that sends current pulses through each motor winding. A popular three-phase full bridge circuit is used to accomplish this by implementing 12 power electronic switches (MOSFETs), as shown in Figure 13. A buck converter is built in front of the bridge circuit for adjusting the amplitude of the PWM wave. Then, the power electronics in the three-phase bridge are responsible only for a few hundred hertz of on-off switching action according to the feedback position signal of the rotor. In this paper, the overall efficiency is increased not only by the optimal phase currents but also by the use of a buck converter, which usually is operated in 5 kHz. Without it, the power electronic components must perform high-frequency (about 20 kHz) switching operations, yielding high switching loss. Additional circuits are also installed, protecting the drive from overload; over-current, over-voltage, over-current, or over-voltage transients; high temperature, etc.

5. Summary and Conclusions

The optimal driving current waveform for a disc-type axial-flux brushless DC wheel motor has been successfully designed. The maximum torque with confined ohmic loss is obtained by driving the motor with the optimal current waveform that is proportional to the magnetic flux variation in the air-gap between the stator and the rotor, which is also proved by the Cauchy-Schwarz inequality. A properly selected

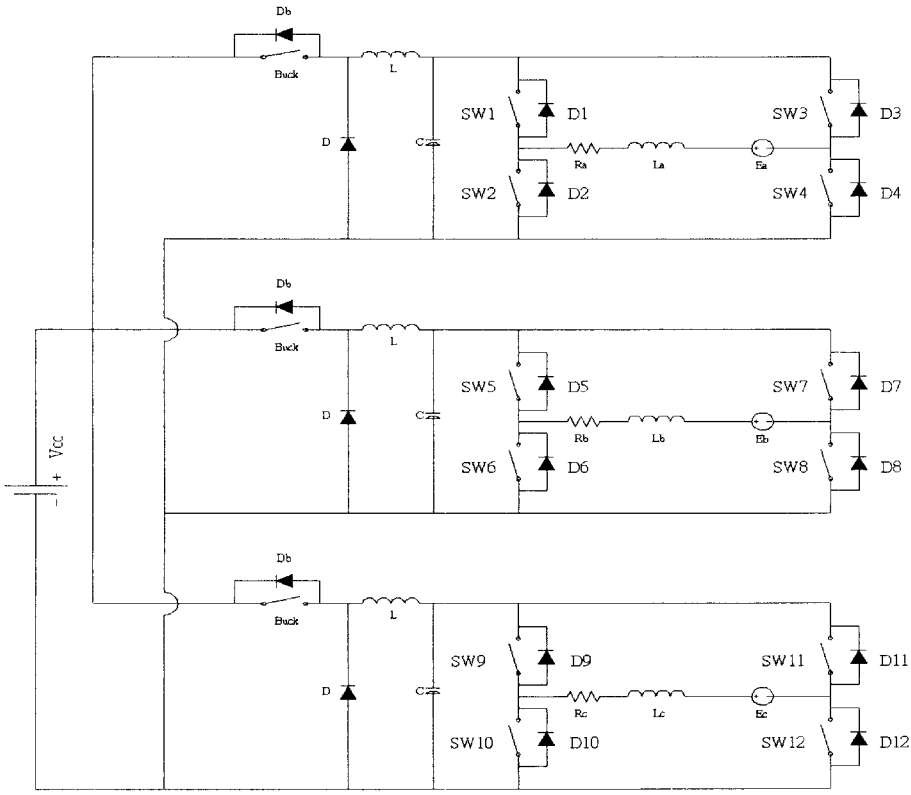

Figure 13. Motor drive for independent winding.

digital signal processor will facilitate the realization of the resulting optimal current and is suggested for further validation through experiments. It is worth mentioning that the procedure of obtaining an optimal current waveform must be applied for most DC brushless motors whose major part of torque stems from the alignment torque due to the mutual flux linking the magnet to the coil.

References

[1] F. Profumo, Z. Zhang, and A. Tenconi, 1997, "Axial Flux Machines Drives: A New Viable Solution for Electric Cars," *IEEE Transactions on Industrial Electronics*, Vol. 44, No. 1, pp. 39–45.

[2] F. Caricchi, F. Crescimbibi, O. Honorati, A. Di Napoli, and E. Santini, 1996, "Compact Wheel Drive for Evs," *IEEE Industry Applications Magazine*, Vol. 2, No. 6, pp. 25–32.

[3] H. C. Lovatt, V. S. Ramsden, and B. C. Mecrow, 1998, "Design of an In-Wheel Motor for a Solar-Powered Electric Vehicles," *IEE Proceedings: Electric Power Applications*, Vol. 145, No. 5, pp. 402–408.

[4] B. Hredzak, S. Gair, and P. Eastham, 1996, "Elimination of Torque Pulsations in a Direct Drive EV Wheel Motor," *IEEE Transactions on Magnetics*, Vol. 32, No. 5, Part 2, pp. 5010–5012.

[5] D. Y. Ohm, 1996, "Optimized Control Method Produces Maximum Torque in PM Synchronous Motors," *Powerconversion & Intelligent Motion*, Vol. 22, No. 8, pp. 30–45.
[6] A. Verl and M. Bodson, 1998, "Torque Maximization for Permanent Magnet Synchronous Motors," *IEEE Transactions on Control System Technology*, Vol. 6, pp. 740–745.
[7] T.-S. Low, C. Bi, and K.-T. Chang, 1996, "Motor Identity—A Motor Model for Torque Analysis and Control," *IEEE Transactions on Industrial Electronics*, Vol. 43, No. 2, pp. 285–291.
[8] C. Mademlis, J. Xypteras, and N. Margaris, 1998, "Loss Minimization in Wound-Field Cylindrical Rotor Synchronous Motor Drives," *IEEE Transactions on Power Electronics*, Vol. 13, No. 2, pp. 288–296.
[9] V. Ostovic, 1994, *Computer-Aided Analysis of Electric Machines*, Prentice Hall, New York.
[10] D. C. Hanselman, 1994, *Brushless Permanent-Magnet Motor Design*, McGraw-Hill, Inc., New York.
[11] E. Kreyszig, 1978, *Introductory Functional Analysis with Applications*, John Wiley & Sons, New York.
[12] G. R. Slemon, 1992, *Electric Machines and Drives*, Addison-Wesley Publishing Company, Inc.